This is a repository copy of *Simultaneous direct visualisation of liquid water in the cathode and anode serpentine flow channels of proton exchange membrane (PEM) fuel cells*.

White Rose Research Online URL for this paper:
https://eprints.whiterose.ac.uk/120643/

Version: Accepted Version

Article:
Aslam, R.M., Ingham, D.B., Ismail, M.S. et al. (3 more authors) (2018) Simultaneous direct visualisation of liquid water in the cathode and anode serpentine flow channels of proton exchange membrane (PEM) fuel cells. Journal of the Energy Institute, 91 (6). pp. 1057-1070. ISSN 1743-9671

https://doi.org/10.1016/j.joei.2017.07.003

Article available under the terms of the CC-BY-NC-ND licence (https://creativecommons.org/licenses/by-nc-nd/4.0/).

Reuse
This article is distributed under the terms of the Creative Commons Attribution-NonCommercial-NoDerivs (CC BY-NC-ND) licence. This licence only allows you to download this work and share it with others as long as you credit the authors, but you can't change the article in any way or use it commercially. More information and the full terms of the licence here: https://creativecommons.org/licenses/

Takedown
If you consider content in White Rose Research Online to be in breach of UK law, please notify us by emailing eprints@whiterose.ac.uk including the URL of the record and the reason for the withdrawal request.

eprints@whiterose.ac.uk
https://eprints.whiterose.ac.uk/

Title

Simultaneous direct visualisation of liquid water in the cathode and anode serpentine flow channels of proton exchange membrane (PEM) fuel cells.

Authors

R. M. Aslam*, D.B. Ingham, M. S. Ismail, K. J. Hughes, L. Ma, M. Pourkashanian

Energy 2050, Department of Mechanical Engineering, Faculty of Engineering, University of Sheffield, Sheffield, S3 7RD, Sheffield. United Kingdom.

*Corresponding author, Tel: +44 114 215 7244

Email address: rmarajaarif1@sheffield.ac.uk (R. M. Aslam)

Abstract

Water flooding is detrimental to the performance of the proton exchange membrane fuel cell (PEMFC) and therefore it has to be addressed. To better understand how liquid water affects the fuel cell performance, direct visualisation of liquid water in the flow channels of a transparent PEMFC is performed under different operating conditions. Two high-resolution digital cameras were simultaneously used for recording and capturing the images at the anode and cathode flow channels. A new parameter extracted from the captured images, namely the wetted bend ratio, has been introduced as an indicator of the amount of liquid water present at the flow channel. This parameter, along with another previously used parameter (wetted area ratio), has been used to explain the variation in the fuel cell performance as the operating conditions of flow rates, operating pressure and relative humidity change. The results have shown that, except for hydrogen flow rate, the wetted bend ratio is strongly linked to the operating condition of the fuel cell; namely: the wetted bend ratio was found to increase with decreasing air flow rate, increasing operating pressure and increasing relative humidity. Also, the status of liquid water at the anode was found to be similar to that at the cathode for most of the cases and therefore the water dynamics at the anode side can also be used to explain the relationships between the fuel cell performance and the investigated operating conditions.

Keywords: PEMFC; Water management; Wetted ratio; Direct visualisation; Operating conditions

1. Introduction

Proton exchange membrane fuel cells (PEMFCs or PEM fuel cell) have a great potential to replace conventional fossil fuel dependent power conversion technologies in a wide range of portable, automotive and stationary applications and this is due to their high efficiency, quick start-up and sizing flexibility [1], [2]. Due to their capability of providing a wide range of energy (from a few watts to MW range), they have been attractive sources of energy for a wide range of portable and mobile applications [3]. However, there are still some challenges that have to be overcome before realising widespread commercialisation of the technology [4]–[6]

Water flooding, especially in the cathode, is one of the main challenges that PEMFC faces and therefore it needs to be addressed [7], [8]. The performance of the PEMFC highly relies on how water is managed within the fuel cell. Namely, the polymeric Nafion membrane needs to be adequately hydrated to conduct protons to the cathode catalyst layer [9]. In other words, a poorly hydrated membrane results in poor protonic conductivity and consequently poor cell performance. Also localised drying of the membrane can occur and may lead to excessive ohmic heating and ultimately pinhole formation in the membrane [10]. On the other hand, it is important not to have 'unnecessary' liquid water at the electrodes to avoid flooding that partially or completely blocks the pathways for the reactant gases to reach the actives sites in the catalyst layers [11].

When studying water management in PEMFCs, the focus is more on the cathode side of the fuel cell as water is produced at the cathode electrode and therefore is more susceptible to water flooding, especially at high current densities [8]. However, the anode side can also be susceptible to water flooding under certain conditions, such as at low current densities and/or with low fuel flow rates [12]. Moreover, the anode gas is generally humidified before entering the fuel cell to prevent the dry-out of the membrane phase at the anode side. Under

certain operating conditions, water vapour condenses, causing water flooding at the anode side [13]. Therefore, to comprehensively address the water management issue in PEMFCs, one needs to investigate both sides of the fuel cell, i.e. the cathode and anode sides.

In order to study the behaviour of water, a visualisation technique has to be employed. Bazylak [14] has listed and reviewed the techniques that have been used to visualise liquid water in PEMFCs, namely: nuclear magnetic resonance (NMR), beam interrogation (Neutron imaging, X-ray and electron microscopy) and optical photography (direct and fluorescence microscopy). In this paper, a direct visualization technique has been used to obtain an understanding of the water behaviour inside the PEMFC due to the advantages of excellent spatial and temporal resolution and its ease to be utilized for the transparent PEMFC. Numerous previous works have been performed experimentally using this technique to visualize the water behaviour and distribution inside the PEMFC.

Notably, most of the visualisation studies have been limited to a qualitative description of liquid water(e.g. mist, droplet, slug and film); see for example [15]–[23]. There were very few investigations that have attempted to provide a quantitative indicator on how flooded are the channels and they are limited to specific PEMFC designs and configuration. Furthermore, the investigations which have simultaneously visualised the cathode and the anode fuel cells under various operating conditions are very few [24]–[27]. Rahimi-Esbo et al. [15] designed a transparent PEM fuel cell to study the water management and contact resistance under dead-end and open-end mode. Bhaskar et al. [16] visualized the water transport mechanisms inside a bio-inspired PEM fuel cell. They found that the bio-inspired fuel cell performed better than the conventional one. However, there is no discussion on the water quantification inside the flow channel. Hussaini et al. [28] visualized water flooding at the cathode using direct optical photography. They introduced a quantitative indicator that has been termed as

the “wetted area ratio”. However, in their investigation, they limited the time of operation to 30 minutes which, as will be seen in the results section, may not be sufficient to reach steady state operation. Yamauchi et al. [29] estimated water content in the flow channels under different levels of humidity using a 3-pass serpentine type flow channel flow configuration. They analysed water flooding phenomena at the anode side and found that it mainly occurs as a result of water diffusion from the cathode electrode to the anode electrode through the membrane under the condition of low humidity. Ous et al. [20] estimated the amount of water in the flow channels at the cathode and anode sides of a transparent PEMFC under different operating conditions. They did so by estimating the contact angles and the diameters of the water droplets through image processing, and subsequently substituting them into Young’s equation to calculate the volume of liquid water. They reported that the air and hydrogen flow rates contributed similarly to the water formation at the cathode channels but differently to the water extraction. Bozorgnezhad et al. [22] investigated two-phase flow in the cathode side at different operating conditions. They focussed on the analysis of the patterns of the two-phase flow (i.e. droplets, film, slug and plug) and how their formations are affected by the operating conditions. Another recent investigation utilizing direct utilization was done by Yuan et al. [27]. They used a direct methanol fuel cell to investigate the effect of different flow fields on the water transport behaviours.

There has been a great deal of research to experimentally and numerically investigate the effects of the operating conditions on the performance of PEMFC [20], [30]–[38]. However, to our knowledge, there has been no investigation that has qualitatively and quantitatively related the operating conditions to water formation and dynamics in both the cathode and anode flow channels in a simultaneous manner. Also, in this work a new parameter, termed as the wetted bend area ratio, has been introduced. This parameter has been used as an indicator

of how flooded are the serpentine flow channels. It is defined as the ratio between the number of the bends flooded with water and the total number of bends in a serpentine flow field channel. As will be shown in the Results and Discussion Section, this is a very good indicator of water flooding in the serpentine flow channels. The formation and accumulation of water was found to be more profound at the bends of the serpentine flow channels and this is mainly due to the relatively large contact area between the water and the walls which subsequently results in an increased water viscosity [39].

Hence in this paper, the newly-introduced parameter, i.e. the wetted bend ratio, will be employed to give an indication on how flooded the flow channels are and subsequently explain the variations in the performance of the fuel cell as the operating conditions of flow rates, operating pressure and relative humidity at both sides change. To achieve this, direct optical photography, which is characterised by excellent spatial and temporal resolution [14], will be employed.

2. Experimental Investigation

2.1 Experimental test setup

All the visualisation experiments were carried out using a commercial transparent PEM fuel cell, CPK202 ClearPak (Pragma Industries). It is a single cell with a single-pass serpentine and the active area is 25 cm^2. The current collectors of the above fuel cell were made from gold plated copper. According to the manufacturer, the catalyst loading is 0.3 mg Pt/cm^2 at the anode and 0.6 mg Pt/cm^2 at the cathode and the electrolyte is Nafion 25 μm. The cell temperature was kept constant at room temperature throughout all the investigation. An in-house fuel cell test station is used to operate the PEMFC, see Fig. 1. The bubble humidifier is used in the fuel cell test station due to its ease of operation. Also, it requires small power consumption and facilitates good control over the relative humidity of the reactant gases.

However, the drawbacks using the bubble humidifier is the gas-vapour mixture can condense along the gas tube before entering the fuel cell. This is prevented by setting the gas temperature higher than the bubble humidier. The humidifier is designed with stainless steel vessel and has a capacity of 0.5 dm^3 water volume, maximum operating pressure to 2.5 bar and operating temperature of 20 to 85 ^oC. The working pressures in the fuel cell test station are controlled by the gas regulators at the inlets and these regulators regulate the high pressure of the gases from the gas sources to a suitable working pressure of fuel cell the test station, namely lower than 2.5 bar and an acceptable operating pressure of the PEM fuel cell. Two back pressure regulators are installed in the fuel cell test station at the gas outlet of the PEM fuel cell and these regulators control the operating pressure inside the PEM fuel cell. The performance of the PEM fuel cell, in the form of potentiostatic, galvanostatic and polarisation curves was captured using GAMRY 3000 coupled with 30k GAMRY booster. In order to simultaneously visualize the formation, accumulation and transport of liquid water in both the cathode and anode flow channels, two high-resolution digital cameras (Casio EX-F1 and Canon EOS 80D) were used.

[Insert Fig. 1 and Fig. 2]

In this study, as mentioned above, a new parameter called the wetted bend ratio is introduced, and the wetted area ratio adopted from [28] is also utilized. Fig. 2 shows a schematic diagram of the experimental setup. Before, we conclude this section, we would like to emphasise that all the experiments were repeated twice in order to confirm the repeatability of the results and the reliability of the findings.

2.2 Wetted bend ratio and wetted area ratio

As mentioned in the introduction, a new parameter extracted from the captured images, the wetted bend ratio has been introduced as an indicator of the amount of liquid water present at the bend of the flow channel. This parameter, along with wetted area ratio [28] will be used to explain the variation in the fuel cell performance as the operating conditions of flow rates, operating pressure and relative humidity change. Wetted bend ratio can be simply calculated by counting the bends that are occupied by liquid water and then dividing them by the total number of bends, i.e. 20. On the other hand, the wetted area ratio is calculated by measuring the total length of the water-covered areas of the channel and then dividing it by the entire length of the channel; see Fig. 3. The estimation of the wetted bend ratio is obviously easier than the estimation of the wetted area ratio. It should be noted that, for simplification, we consider the bend or the portion of the channel wet when there exists a considerable amount of liquid water in these regions.

[Insert Fig. 3]

3. Results and discussion

3.1 Effect of gas flow rates

Two sets of experiments were carried out to study the effect of gas flow rates on the PEMFC performance and the status of liquid water in the flow channel. The flow rates of the supplied gas into the PEM fuel cell are controlled by the mass flow controllers (Teledyne Hasting Instrument, HFC 202) which are installed in the test station before the gas inlets of the PEM fuel cell. The first set of experiments is concerned with the effects of the air flow rate; the set of air flow rates used were: 0.10, 0.15, 0.20 and 0.25 Standard Litre per Minute (SLPM) while the hydrogen flow rate has been kept constant at 0.05 SLPM which is the theoretical

hydrogen flow rate calculated based on a total current of 8 A and stoichiometric ratio of about 1.5. The second set of experiments is concerned with the effects of the hydrogen flow rate; the set of hydrogen flow rates used were: 0.03, 0.05, 0.07 and 0.09 SLPM while the air flow rate has been kept constant at 0.20 SLPM which is the theoretical air flow rate calculated based on a total current of 8 A and stoichiometric ratio of about 1.3. During the experiments, the operating conditions of temperature, pressure and relative humidity, were kept constant. The gas inlet temperature and pressure on both sides were at room temperature and 1 barg, respectively. The anode and cathode gas relative humidity were recorded by humidity sensor (Hygroflex Rotronic, Switzerland) as 75% and 85%, respectively. The polarization and potentiostatic curves of each set of experiments have been recorded. Images for the cathode and anode flow channel for each case were taken from the recording at the same moment to examine the status of the liquid water at both sides simultaneously.

Fig. 4(a) shows the polarization curves for the cases in which the air flow rate has been changed from 0.10 to 0.25 SLPM. In general, the fuel cell performance improves as the air flow rate increases from 0.10 to 0.20 SLPM. When increased to 0.25 SLPM, the fuel cell performance has been, compared to 0.15 and 0.20 SLPM cases, found to be lower for the cell potentials above 0.60 V. However, the flow rate of 0.25 SLPM was shown to give the highest limiting current density amongst the investigated cases.

Based on the above, one can see that, for the given operating conditions, there exists an optimum air flow rate, 0.20 SLPM. The air flow rates 0.10 and 0.15 SLPM appear to be not sufficiently high to drive the excess liquid water away from the flow channel, thus causing undesirable water accumulation that limits the performance of the fuel cell at relatively high current densities. On the other hand, the air flow rate 0.25 SLPM appears to be so high, affecting the level of hydration needed for the membrane. These findings will be confirmed

later in this section through the recorded images of the flow channels and the calculated water ratio numbers.

To investigate the status of the liquid water in the flow channels, the potentiostatic curves were generated at 0.70 V which was found to be the minimum reasonable cell voltage for all the cases before the introduction of the mass transport losses, see Fig. 4(b). As with the corresponding polarization curves, it can be seen that, after reaching almost the 'pseudo' steady-state condition, the best fuel cell performance is when the air flow rate is 0.20 SLPM and is the worst when the air flow rate is 0.10 SLPM.

The wetted bend ratio and wetted area ratio for both sides have been calculated from the captured images and plotted in Fig. 5. It can be seen that they both decrease as the air flow rate increases. As indicated earlier, this is most likely to be due to the increase in the ability to remove liquid water from the flow channel with increasing air flow rate. Since water is produced at the cathode, the wetted ratio numbers at the anode are smaller than those of the cathode. However, their trends are similar to each other even though the hydrogen flow rate has been kept constant. This may be attributed to the net water transport across the membrane through the electro-osmotic drag and the back diffusion. This indicates that the wetted ratio numbers at the anode side can also be employed to interpret the relationship between the fuel cell performance and the air flow rate.

[Insert Fig. 4 and Fig. 5]

Fig. 6(a) shows the polarization curves for the cases in which the hydrogen flow rate has been changed from 0.03 to 0.09 SLPM. It can be seen from the figure that the hydrogen flow rate of 0.07 SLPM gives the maximum limiting current density amongst all the investigated cases; this is probably due to the observation that the number of flooded bends in this case is the minimum (see Fig. 7a). Also, the hydrogen flow rate of 0.03 and, to a less extent, 0.05 SLPM appear to be insufficient to maintain the fuel cell operating after 100 and 200 mA/cm^2,

respectively. Further, ignoring the limiting current densities, the best performance was shown when the fuel cell was supplied with 0.05 SLPM hydrogen gas. As with the cathode side, the potentiostatic curves for all the cases were recorded at 0.70 V in order to investigate the status of the liquid water in the flow channels, see Fig. 6(b). In accordance with the polarization curves at 0.70 V, the highest current density, at pseudo steady-state conditions, was shown when the fuel cell was run with a hydrogen flow rate of 0.05 SLPM and the lowest current density was when it was run with a hydrogen flow rate of 0.07 SLPM.

Fig. 7 show the wetted ratio numbers calculated for the cathode and anode flow channels at 0.70 V for the cases in which hydrogen flow rate has been changed from 0.03 to 0.09 SLPM. The wetted ratio numbers at the cathode, (Fig. 7(a)) can be somewhat related to the trends shown in the potentiostatic curves, see Fig. 6(b): the larger is the current density at 0.70 V, the higher are the wetted ratio numbers (either for the entire channel or the bends) at the cathode side. This is expected since more water is generated as the current produced increases. However, there are almost no apparent trends that can be deduced from the wetted ratio numbers at the anode side (Fig. 7(b)) as the hydrogen flow rate increases; the wetted bend ratio is the same for all the flow rates and the change of the wetted area ratio with the hydrogen flow rate is almost negligible.

Overall, for all the given operating conditions mentioned earlier, the optimum hydrogen flow rate at 0.70 V is 0.05 SLPM. It is not very clear why the current density is at a maximum with 0.05 SLPM hydrogen flow rate at 0.70 V; it may be the flow rate that supplies a sufficient amount of hydrogen to the anode electrode without removing away a substantial amount of water from the entire membrane electrode assembly (MEA).

As a general observation, the wetted ratio numbers calculated for the bends in all the previous cases are larger than those calculated for the entire channel. This is, as explained in the introduction, attributed to the ease of accumulation of liquid water at the bends. This new

finding gives an insight of how the water behaviour inside the flow field specifically for serpentine channel and give an additional information from the previous works done by other researchers [26], [28].

[Insert Fig. 6 and Fig. 7]

3.2 Effect of operating pressure

The effect of operating pressure on the fuel cell performance has been investigated. The set of pressures investigated were 0, 0.5, 1.0 and 1.5 barg on both cathode and anode sides. It should be noted that 0 barg means that the back-pressure regulator has been set to 0 and consequently there is hardly any increase in the gauge pressure of the fuel cell. The effect of the pressure has been demonstrated in the form of the polarization and galvanostatic curve, see Fig. 8. The galvanostatic test, rather than the potentiostatic test, has been adopted in this investigation as it was shown to give more stable readings with this investigation. A constant current of 2.5 A has been set when performed the galvanostatic test.

As with the previous investigation of flow rates, all the other parameters were kept constant. The flow rate of air and hydrogen were 0.20 and 0.05 SLPM, respectively. From Fig. 8, one can see that the fuel cell performance in general enhances as the operating pressure increases as reported by other previous findings [35], [40]. This is attributed to the increase in the partial pressure of the reacting gases (e.g air and hydrogen) which subsequently increases the open circuit (or the starting) potential of the fuel cell; this is evident from the Nernst equation which is used to calculate the maximum open circuit potential [41]. Also, it can be noted that as the current density increases; the polarization curves of 0.5 and 1.5 barg approach those of 0 and 1.0 barg, respectively. This could be explained by the increase in the mass transport losses in the former two cases, i.e. 0.5 and 1.5 barg, due to the increase of the amount of water generated at relatively high current densities.

Fig. 9 show the wetted ratio numbers calculated for the cathode and the anode flow channels at 2.5 A for the cases in which the operating pressure has been changed from 0 to 1.5 barg. It can be seen from the graphs that the wetted ratio numbers increase as the operating pressure increases. As the current has been kept constant, the amount of water generated is the same for all cases. However, it is well-known that as the operating pressure, controlled by a backpressure regulator, decreases, the ability to purge liquid water from the flow channel increases.

As with the previous investigation, the similarity of the trends of the wetted ratio numbers at both the cathode and the anode indicates that these numbers at the anode side can also be employed to interpret the relationship between the fuel cell performance and the operating pressure of the fuel cell.

[Insert Fig. 8 and Fig. 9]

3.3 Effect of relative humidity

The effect of inlet relative humidity on the fuel cell performance has also been investigated. To achieve this, the hydrogen has been kept dry while investigating the effect of the inlet relative humidity of air and vice versa. The relative humidity data is changed by changing the temperature of the bubble humidifier while keeping the temperature of the inlet gas constant. Tables 1 and 2 list the values of the inlet relative humidity used for the cathode and anode sides respectively.

[Insert Table 1 and Table 2]

Fig. 10 shows the polarization and potentiostatic curves for the cases in which the relative humidity of air has been varied to investigate its effects. It can be seen from the polarization curves (Fig. 10(a)), of all the conditions investigated, the optimum fuel cell performance was obtained at an air relative humidity of 88%; it might be the trade-off value (amongst the

investigated values) between the positive effect of membrane hydration and negative effect of water accumulation. As expected the wetted ratio numbers at the cathode side increase as air relative humidity increases, see Fig. 11(a). A similar trend is shown at the anode side and this is due to the diffusion of water from the cathode to the anode, see Fig. 11(b).

Fig. 12 shows the polarization and potentiostatic curves for the cases in which the relative humidity of hydrogen has been varied to investigate its effect. One can clearly see that the fuel cell performance for all the investigated cases is relatively low. This could be attributed to the use of dry air. Also, it can be observed that the fuel cell performance increases as the hydrogen relative humidity increases, leading to better membrane hydration and enhanced ionic conductivity. Notably, the potentiostatic curves of the cases, at 0.70 V, are highly erratic. This is apparently due to the high dynamics of liquid water at the anode side which has been confirmed through the corresponding recordings. However, towards the end of the timeline, the order of the cases in terms of the current density has been in line that of the polarization curve at 0.70 V.

Fig. 13 show the wetted ratio numbers calculated for the cathode and the anode flow channels at 0.70 V for the cases in which the hydrogen relative humidity has been changed from 10 to 100%. As expected, the wetted ratio numbers increase as the relative humidity of hydrogen increases.

As with the previous investigation, the similarity of the trends of the wetted ratio numbers at both the cathode and the anode indicates that these numbers at the anode side can also be used to interpret the relationship between the fuel cell performance and the relative humidity of the inlet gases.

[Insert Fig. 10, Fig. 11, Fig. 12 and Fig. 13]

4. Conclusions

In this paper, a direct visualisation of flow channels at both the cathode and anode of a transparent PEM fuel cell has been performed simultaneously. A new parameter, wetted bend ratio, which gives an indication of how the bends of the serpentine flow channels are flooded, has been introduced. It has been used to elucidate the variation in the fuel cell performance as a number of operating conditions (i.e. the flow rates, the operating pressure and the relative humidity) are changed. The following are the main findings:

- There exist optimum values for the air and hydrogen flow rates. These values form the trade-off between the positive effect of purging the liquid water from the flow channel and the negative effect of the membrane dry-out.
- As the operating pressure increases, the fuel cell performance and the wetted bend ratio increase.
- There exists an optimum value for the air relative humidity which is the trade-off between the positive effect of membrane hydration and negative effect of water flooding. On the other hand, the fuel cell performance was found to increase with increasing hydrogen relative humidity. As expected, the wetted bend ratio was found to increase as the relative humidity of either air or hydrogen increases.
- In most of the investigations, it has been shown that the trends of wetted ratio numbers for both the cathode and anode have been similar. This implies that the anode side, where there is no water production, can also be used to explain the relationship between the fuel cell performance and the operating conditions.

Acknowledgements

The first author gratefully acknowledged the Malaysia Government through MARA Education Fund, Malaysia for the funding and the technical assistance from Mr. Dmitry Govorukhin.

References

[1] C. Dyer, “Fuel cells for portable applications,” *Fuel Cells Bull.*, no. 42, pp. 9–10, 2002.

[2] E. Carcadea, H. Ene, D. B. Ingham, R. Lazar, L. Ma, M. Pourkashanian, and I. Stefanescu, “A computational fluid dynamics analysis of a PEM fuel cell system for power generation,” *Int. J. Numer. Methods Heat Fluid Flow*, vol. 17, no. 3, pp. 302–312, 2007.

[3] M. S. Ismail, T. Damjanovic, K. Hughes, D. B. Ingham, L. Ma, M. Pourkashanian, and M. Rosli, “Through-Plane Permeability for Untreated and PTFE-Treated Gas Diffusion Layers in Proton Exchange Membrane Fuel Cells,” *J. Fuel Cell Sci. Technol.*, vol. 7, no. 5, p. 51016, 2010.

[4] K. Sopian and W. R. Wan Daud, “Challenges and future developments in proton exchange membrane fuel cells,” *Renew. Energy*, vol. 31, no. 5, pp. 719–727, Apr. 2006.

[5] L. M. and M. P. M.S. Ismail, K.J. Hughes, D.B. Ingham, “Effect of PTFE loading of gas diffusion layers on the performance of proton exchange membrane fuel cells running at high-efficiency operating conditions,” *Int. J. ENERGY Res.*, 2012.

[6] A. El-kharouf, A. Chandan, M. Hattenberger, and B. G. Pollet, “Proton exchange membrane fuel cell degradation and testing: review,” *J. Energy Inst.*, vol. 85, no. 4, pp. 188–200, 2012.

[7] K. Jiao and X. Li, “Water transport in polymer electrolyte membrane fuel cells,” *Prog. Energy Combust. Sci.*, vol. 37, no. 3, pp. 221–291, Jun. 2011.

[8] H. Li, Y. Tang, Z. Wang, Z. Shi, S. Wu, D. Song, J. Zhang, K. Fatih, J. Zhang, H. Wang, Z. Liu, R. Abouatallah, and A. Mazza, "A review of water flooding issues in the proton exchange membrane fuel cell," *J. Power Sources*, vol. 178, no. 1, pp. 103–117, Mar. 2008.

[9] M. S. Ismail, D. Borman, T. Damjanovic, D. B. Ingham, and M. Pourkashanian, "On the through-plane permeability of microporous layer-coated gas diffusion layers used in proton exchange membrane fuel cells," *Int. J. Hydrogen Energy*, vol. 36, no. 16, pp. 10392–10402, 2011.

[10] H. K. Atiyeh, K. Karan, B. Peppley, A. Phoenix, E. Halliop, and J. Pharoah, "Experimental investigation of the role of a microporous layer on the water transport and performance of a PEM fuel cell," *J. Power Sources*, vol. 170, no. 1, pp. 111–121, Jun. 2007.

[11] K. Jiao, J. Park, and X. Li, "Experimental investigations on liquid water removal from the gas diffusion layer by reactant flow in a PEM fuel cell," *Appl. Energy*, vol. 87, no. 9, pp. 2770–2777, 2010.

[12] J. O'Rourke, M. Ramani, and M. Arcak, "In situ detection of anode flooding of a PEM fuel cell," *Int. J. Hydrogen Energy*, vol. 34, no. 16, pp. 6765–6770, 2009.

[13] S. Ge and C.-Y. Wang, "Liquid Water Formation and Transport in the PEFC Anode," *J. Electrochem. Soc.*, vol. 154, no. 10, p. B998, 2007.

[14] a. Bazylak, "Liquid water visualization in PEM fuel cells: A review," *Int. J. Hydrogen Energy*, vol. 34, no. 9, pp. 3845–3857, May 2009.

[15] A. Ramiar, A. A. Ranjbar, and E. Alizadeh, "ScienceDirect Design , manufacturing , assembling and testing of a transparent PEM fuel cell for investigation of water

management and contact resistance at dead-end mode," *Int. J. Hydrogen Energy*, vol. 42, no. 16, pp. 11673–11688, 2017.

[16] B. P. Saripella, U. O. Koylu, and M. C. Leu, "Experimental and Computational Evaluation of Performance and Water Management Characteristics of a Bio-Inspired Proton Exchange Membrane Fuel Cell," *J. Fuel Cell Sci. Technol.*, vol. 12, no. 6, p. 61007, 2015.

[17] P. Quan, B. Zhou, A. Sobiesiak, and Z. Liu, "Water behavior in serpentine micro-channel for proton exchange membrane fuel cell cathode," *J. Power Sources*, vol. 152, no. 1–2, pp. 131–145, 2005.

[18] T. Ous and C. Arcoumanis, "Visualisation of water droplets during the operation of PEM fuel cells," *J. Power Sources*, vol. 173, no. 1, pp. 137–148, 2007.

[19] E. Kimball and T. Whitaker, "Drops, slugs, and flooding in polymer electrolyte membrane fuel cells," *AIChE*, vol. 54, no. 5, 2008.

[20] T. Ous and C. Arcoumanis, "Visualisation of water accumulation in the flow channels of PEMFC under various operating conditions," *J. Power Sources*, vol. 187, pp. 182–189, 2009.

[21] Z. Lu, S. G. Kandlikar, C. Rath, M. Grimm, W. Domigan, a. D. White, M. Hardbarger, J. P. Owejan, and T. a. Trabold, "Water management studies in PEM fuel cells, Part II: Ex situ investigation of flow maldistribution, pressure drop and two-phase flow pattern in gas channels," *Int. J. Hydrogen Energy*, vol. 34, no. 8, pp. 3445–3456, May 2009.

[22] A. Bozorgnezhad, M. Shams, H. Kanani, M. Hasheminasab, and G. Ahmadi, "Two-phase flow and droplet behavior in microchannels of PEM fuel cell," *Int. J. Hydrogen*

Energy, vol. 41, no. 42, pp. 1–18, 2016.

[23] M. I. Rosli, D. J. Borman, D. B. Ingham, M. S. Ismail, L. Ma, and M. Pourkashanian, "Transparent PEM Fuel Cells for Direct Visualization Experiments," *J. Fuel Cell Sci. Technol.*, vol. 7, no. 6, p. 61015, 2010.

[24] D. Spernjak, A. K. Prasad, and S. G. Advani, "Experimental investigation of liquid water formation and transport in a transparent single-serpentine PEM fuel cell," *J. Power Sources*, vol. 170, no. 2, pp. 334–344, Jul. 2007.

[25] M. M. Daino, Z. Lu, J. M. LaManna, J. P. Owejan, T. a. Trabold, and S. G. Kandlikar, "Through-Plane Water Transport Visualization in a PEMFC by Visible and Infrared Imaging," *Electrochem. Solid-State Lett.*, vol. 14, no. 6, p. B51, 2011.

[26] J. M. Sergi and S. G. Kandlikar, "Quantification and characterization of water coverage in PEMFC gas channels using simultaneous anode and cathode visualization and image processing," *Int. J. Hydrogen Energy*, vol. 36, no. 19, pp. 12381–12392, Sep. 2011.

[27] W. Yuan, A. Wang, Z. Yan, Z. Tan, Y. Tang, and H. Xia, "Visualization of two-phase flow and temperature characteristics of an active liquid-feed direct methanol fuel cell with diverse flow fields," *Appl. Energy*, vol. 179, pp. 85–98, 2016.

[28] I. S. Hussaini and C.-Y. Wang, "Visualization and quantification of cathode channel flooding in PEM fuel cells," *J. Power Sources*, vol. 187, no. 2, pp. 444–451, Feb. 2009.

[29] M. Yamauchi, K. Sugiura, T. Yamauchi, T. Taniguchi, and Y. Itoh, "Proposal for an optimum water management method using two-pole simultaneous measurement," *J. Power Sources*, vol. 193, no. 1, pp. 1–8, 2009.

[30] E. Afshari, M. Ziaei-Rad, and M. M. Dehkordi, “Numerical investigation on a novel zigzag-shaped flow channel design for cooling plates of PEM fuel cells,” *J. Energy Inst.*, pp. 1–12, 2016.

[31] G.-L. Hu, J.-R. Fan, and Y.-Q. Zheng, “CFD based two-phase modelling of proton exchange membrane fuel cell with interdigitated flow field,” *J. Energy Inst.*, vol. 83, no. 2, pp. 93–100, 2002.

[32] S. Patel, A. S. Bansode, T. Sundararajan, and S. K. Das, “The Performance Analysis of a Multi-Duct Proton Exchange Membrane Fuel Cell Cathode,” *Int. J. Green Energy*, vol. 5, no. 1–2, pp. 35–54, 2008.

[33] M. Tohidi, S. H. Mansouri, and H. Amiri, “Effect of primary parameters on the performance of PEM fuel cell,” *Int. J. Hydrogen Energy*, vol. 35, no. 17, pp. 9338–9348, Sep. 2010.

[34] Y. H. Park and J. A. Caton, “Monitoring an Electrode Flooding Through the Back Pressure in a Proton Exchange Membrane (PEM) Fuel Cell,” *Int. J. Green Energy*, vol. 5, no. 5, pp. 347–359, 2008.

[35] J. Zhang, C. Song, J. Zhang, R. Baker, and L. Zhang, “Understanding the effects of backpressure on PEM fuel cell reactions and performance,” *J. Electroanal. Chem.*, vol. 688, pp. 130–136, 2013.

[36] J. Zhang, H. Li, Z. Shi, and J. Zhang, “Effects of Hardware Design and Operation Conditions on PEM Fuel Cell Water Flooding,” *Int. J. Green Energy*, vol. 7, no. 5, pp. 461–474, 2010.

[37] A. Bozorgnezhad, M. Shams, H. Kanani, M. Hasheminasab, and G. Ahmadi, “The experimental study of water management in the cathode channel of single-serpentine

transparent proton exchange membrane fuel cell by direct visualization," *Int. J. Hydrogen Energy*, vol. 40, no. 6, pp. 2808–2832, 2015.

[38] G. Hu, G. Li, Y. Zheng, Z. Zhang, and Y. Xu, "Optimization and parametric analysis of PEMFC based on an agglomerate model for catalyst layer," *J. Energy Inst.*, vol. 87, no. 2, pp. 163–174, 2014.

[39] a Su, F. Weng, C. Hsu, and Y. Chen, "Studies on flooding in PEM fuel cell cathode channels," *Int. J. Hydrogen Energy*, vol. 31, no. 8, pp. 1031–1039, Jul. 2006.

[40] M. Amirinejad, S. Rowshanzamir, and M. H. Eikani, "Effects of operating parameters on performance of a proton exchange membrane fuel cell," *J. Power Sources*, vol. 161, no. 2, pp. 872–875, Oct. 2006.

[41] F. Barbir, *PEM Fuel Cells : Theory and Practice ACADEMIC PRESS*. Elsevier Academic Press, 2005.

[42] Pragma-industries.com. ClearPack Single Cells- Pragma Industries, http://www.pragma-industries.com/products/lab-equipment/clearpak, accessed 18 July 2017.

Figures Captions

Fig. 1 Photograph of the in-house fuel cell test station.

Fig. 2 Schematic diagram of the experimental setup used to visualize the liquid water.

Fig. 3 (a) A photo of the used transparent fuel cell showing the number of the total bends, i.e. 20 [42] and (b) an image that shows how wetted areas in the flow channel.

Fig. 4(a) The polarization curves for all the investigated air flow rates, and (b) the measured current density at 0.70 V as a function of time for all the investigated air flow rates.

Fig. 5 (a) The captured images and the wetted area and bend ratio numbers for the cathode side, and b) the wetted area and bend ratio numbers for the anode side

Fig. 6(a) The polarization curves for all the investigated hydrogen flow rates, and (b) the measured current density at 0.70 V as a function of time for all the investigated hydrogen flow rates.

Fig. 7 The wetted area and bend ratio numbers for the (a) cathode and (b) anode sides.

Fig. 8(a) The polarization curves for all the investigated operating pressures, and (b) the measured cell potential at 2.5 A as a function of time for all the investigated operating pressures.

Fig. 9 The wetted area and bend ratio numbers for the (a) cathode and (b) anode sides.

Fig. 10(a) The polarization curves for all the investigated air relative humidity, and (b) the measured current density at 0.70 V as a function of time for all the investigated air relative humidity.

Fig. 11 The wetted area and bend ratio numbers for the (a) cathode and (b) anode sides.

Fig. 12(a) The polarization curves for all the investigated hydrogen relative humidity, and (b) the measured current density at 0.70 V as a function of time for all the investigated hydrogen relative humidity.

Fig. 13 The wetted area and bend ratio numbers for the (a) cathode and (b) anode sides.

Table 1 Cathode inlet relative humidity for various temperatures of the cathode bubble humidifier and a constant inlet air temperature of 45°C.

Bubble Humidifier Temperature (^{0}C)	Relative Humidity (%)
30	10
40	40
50	88
60	95

Table 2 Anode inlet relative humidity for various temperatures of the anode bubble humidifier and a constant inlet hydrogen temperature of 30°C.

Bubble Humidifier Temperature (°C)	Relative Humidity (%)
40	10
50	20
55	35
60	48
70	100

Fig. 1


Gas regulator
Relative humidity sensor
Humidifier
Relative humidity power unit
PEM fuel cell
Backpressure regulator
Mass flow sensor
Mass flow controller
Flow controller power unit
Differential pressure transducer

Fig. 2

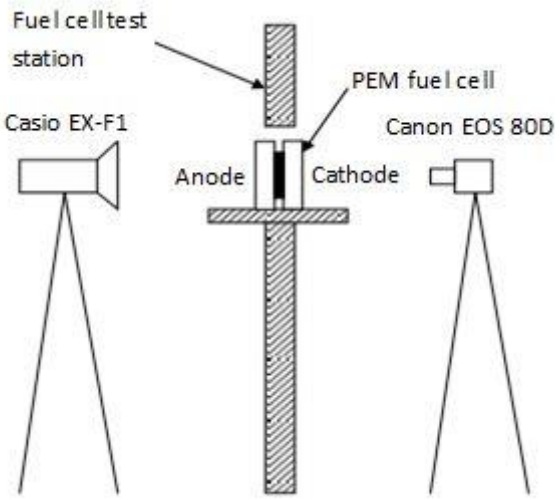
Fuel cell test station
PEM fuel cell
Casio EX-F1
Canon EOS 80D
Anode
Cathode

Fig. 3(a)

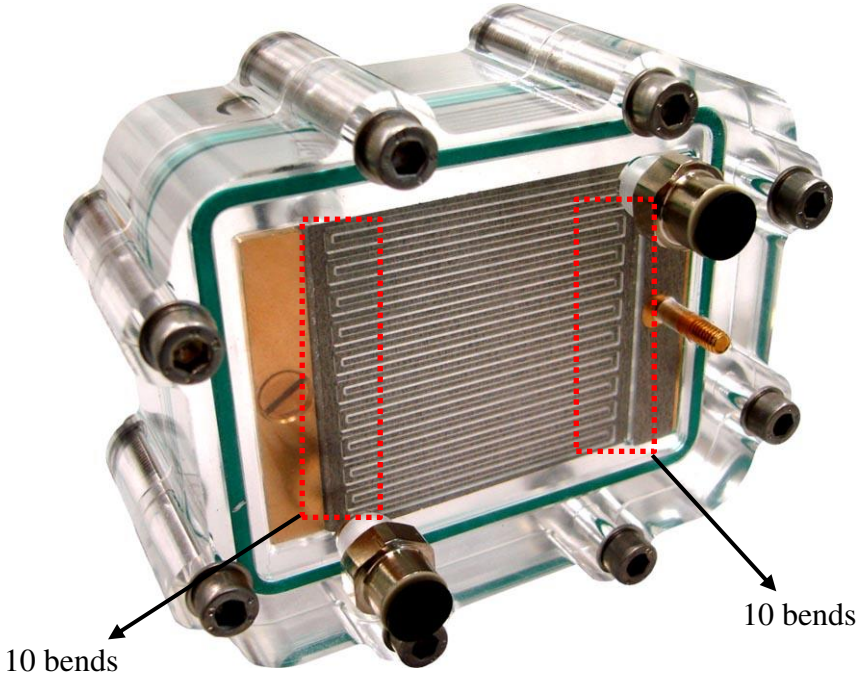

Fig. 3(b)

Fig. 4(a)

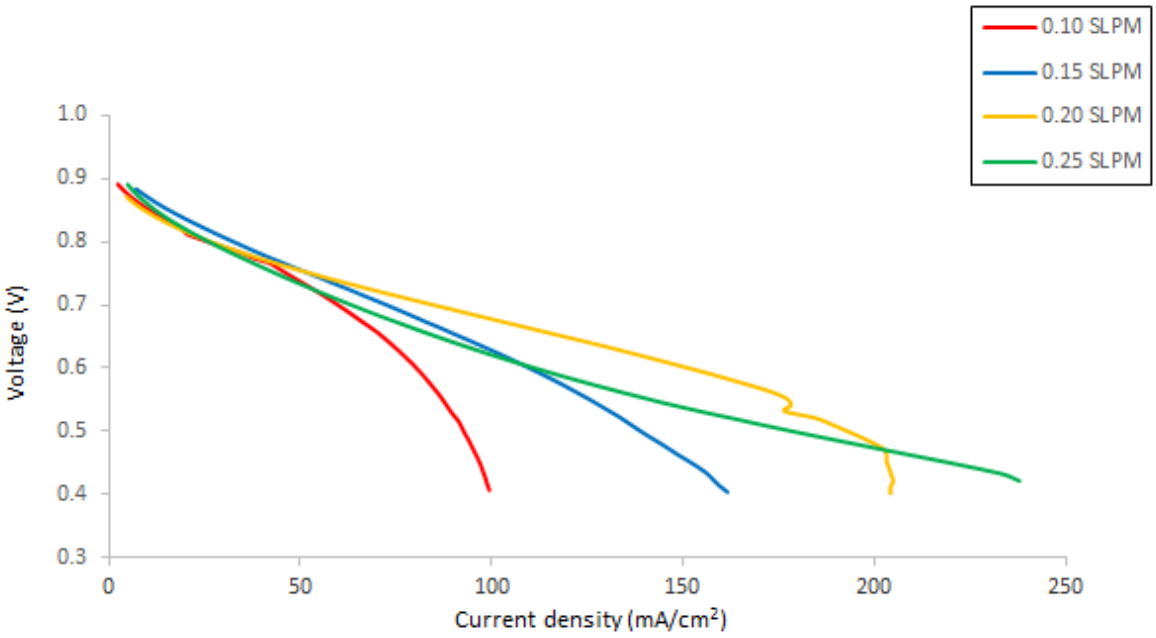
0.10 SLPM
0.15 SLPM
0.20 SLPM
0.25 SLPM
1.0
0.9
0.8
0.7
0.6
0.5
0.4
0.3
Voltage (V)
0
50
100
150
200
250
Current density (mA/cm²)

Fig. 4(b)

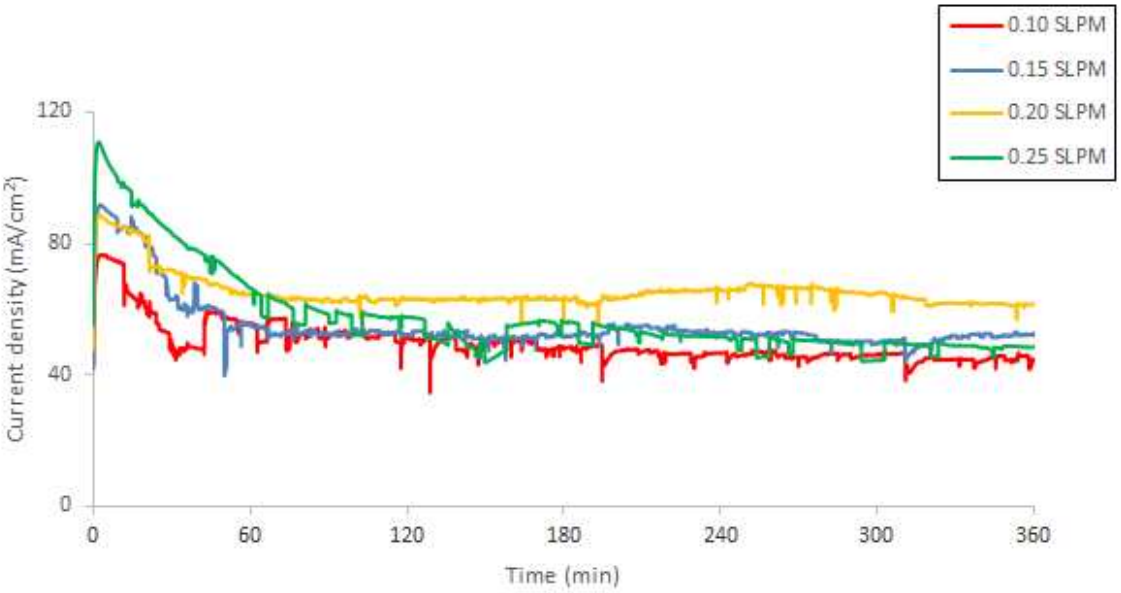
0.10 SLPM
0.15 SLPM
0.20 SLPM
0.25 SLPM
120
80
40
0
Current density (mA/cm²)
0
60
120
180
240
300
360
Time (min)

Fig. 5(a)

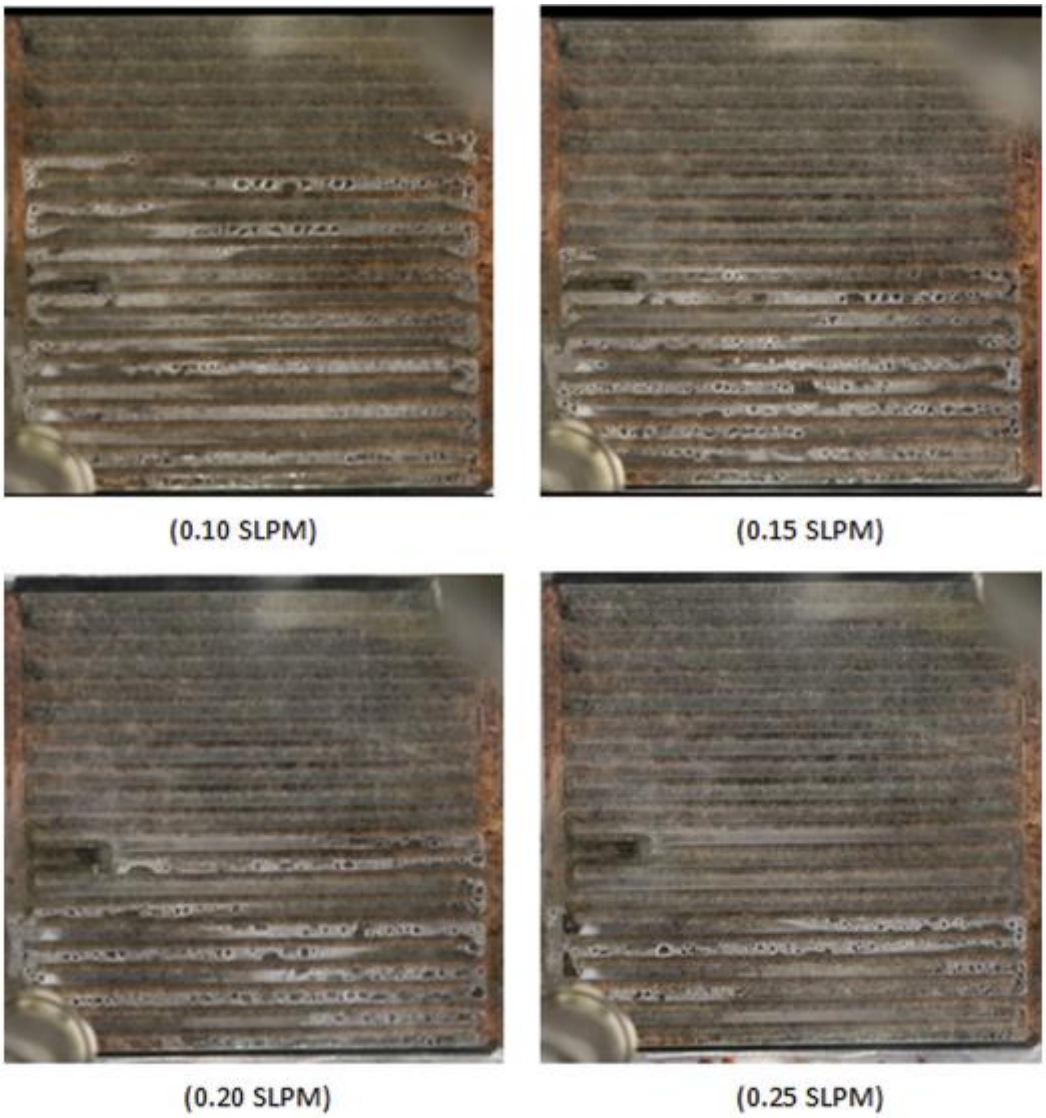
(0.10 SLPM)
(0.15 SLPM)
(0.20 SLPM)
(0.25 SLPM)

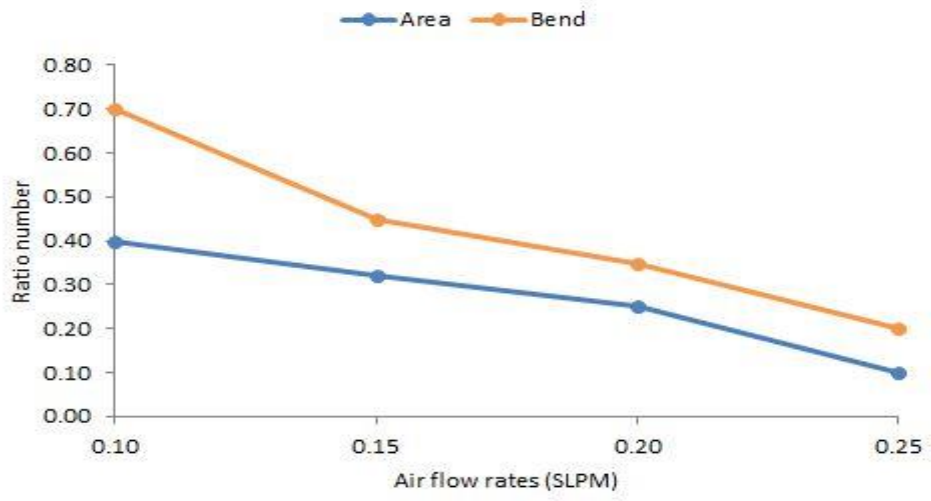
Area
Bend
0.80
0.70
0.60
0.50
0.40
0.30
0.20
0.10
0.00
Ratio number
0.10
0.15
0.20
0.25
Air flow rates (SLPM)

Fig. 5(b)

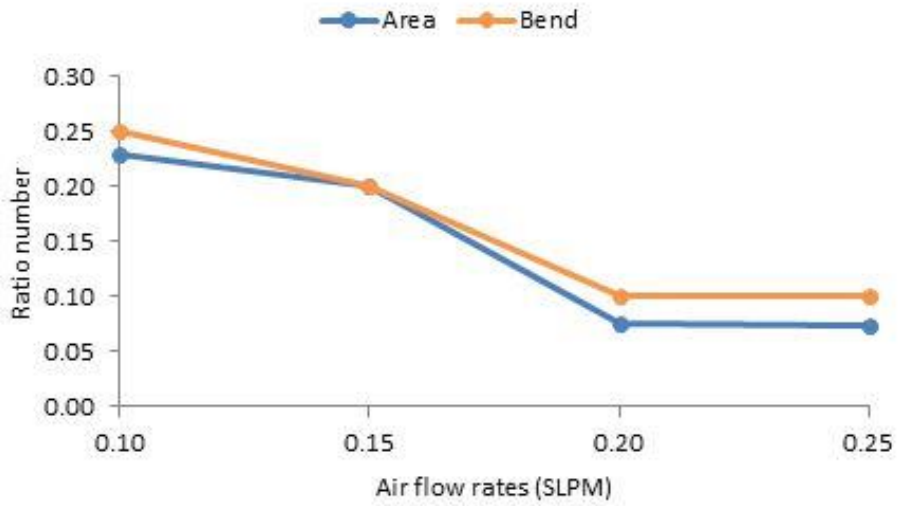
Area
Bend
0.30
0.25
0.20
0.15
0.10
0.05
0.00
Ratio number
0.10
0.15
0.20
0.25
Air flow rates (SLPM)

Fig. 6(a)

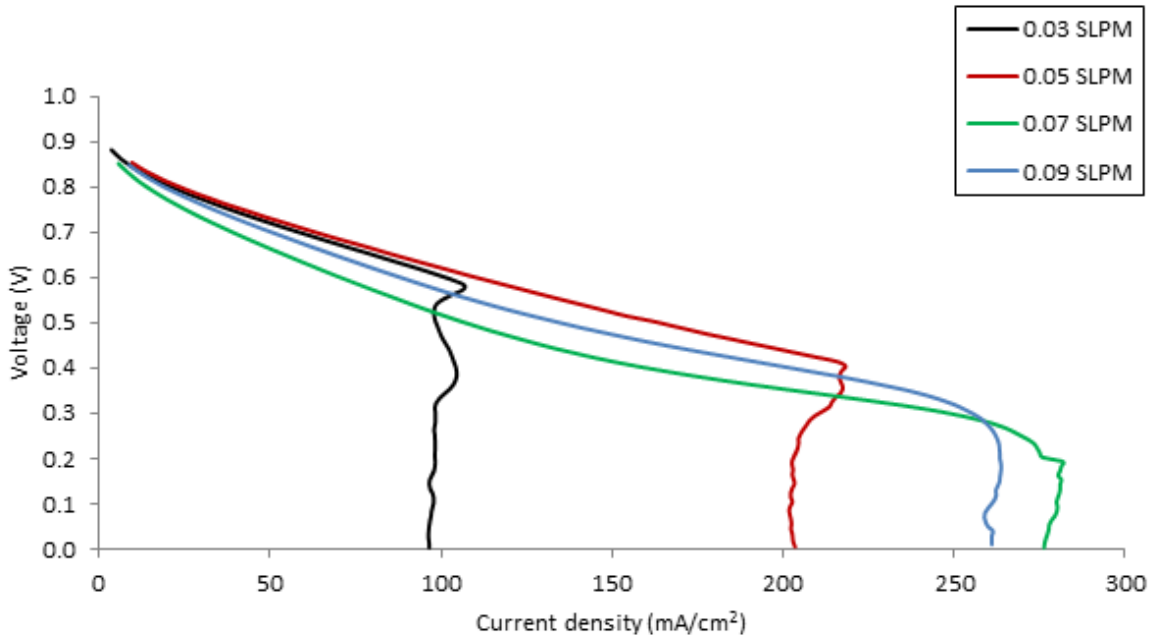
0.03 SLPM
0.05 SLPM
0.07 SLPM
0.09 SLPM
Voltage (V)
1.0
0.9
0.8
0.7
0.6
0.5
0.4
0.3
0.2
0.1
0.0
0
50
100
150
200
250
300
Current density (mA/cm²)

Fig. 6(b)

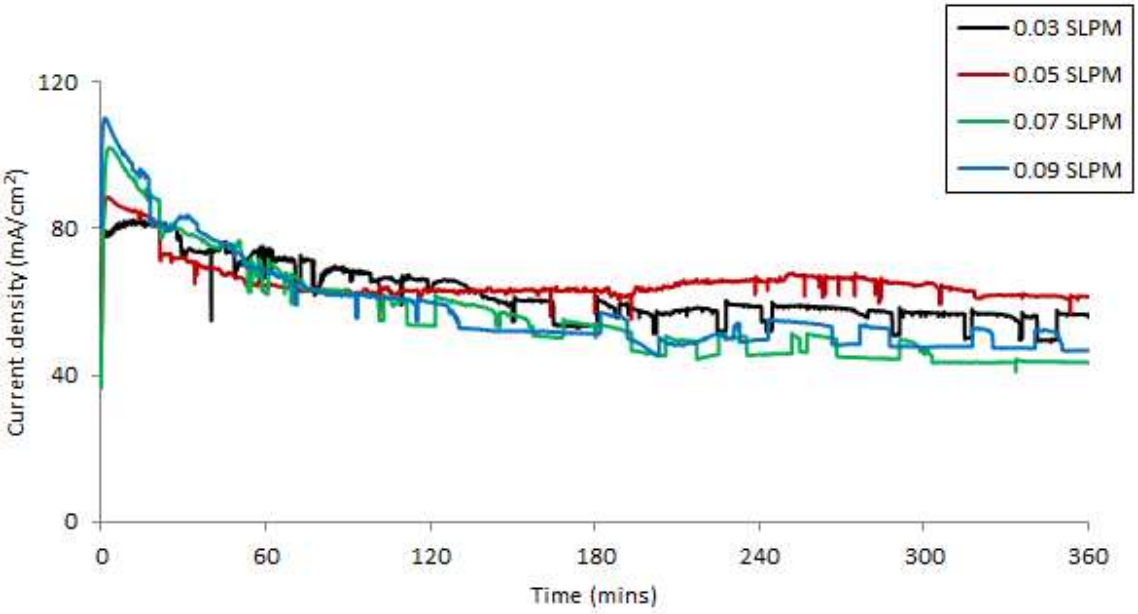
0.03 SLPM
0.05 SLPM
0.07 SLPM
0.09 SLPM
120
80
40
0
Current density (mA/cm²)
0
60
120
180
240
300
360
Time (mins)

Fig. 7(a)

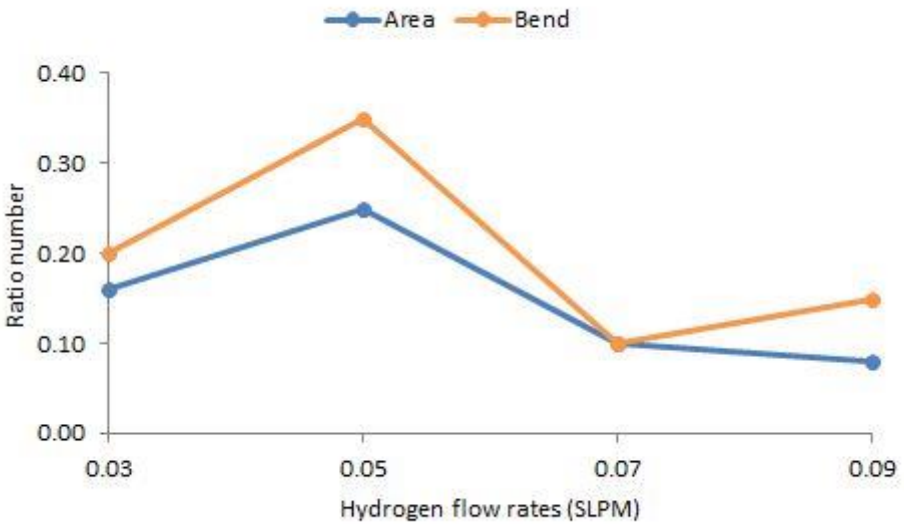
Area
Bend
0.40
0.30
0.20
0.10
0.00
Ratio number
0.03
0.05
0.07
0.09
Hydrogen flow rates (SLPM)

Fig. 7(b)

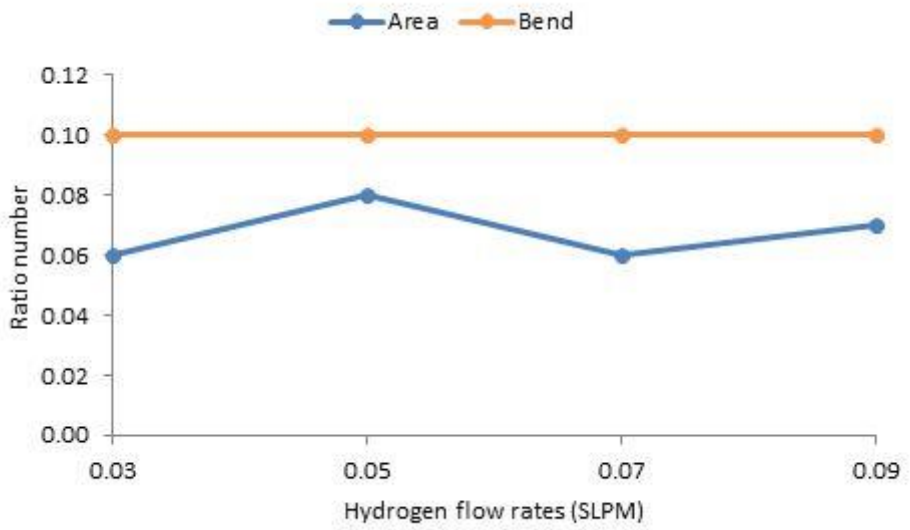
Area
Bend
0.12
0.10
0.08
0.06
0.04
0.02
0.00
Ratio number
0.03
0.05
0.07
0.09
Hydrogen flow rates (SLPM)

Fig. 8(a)

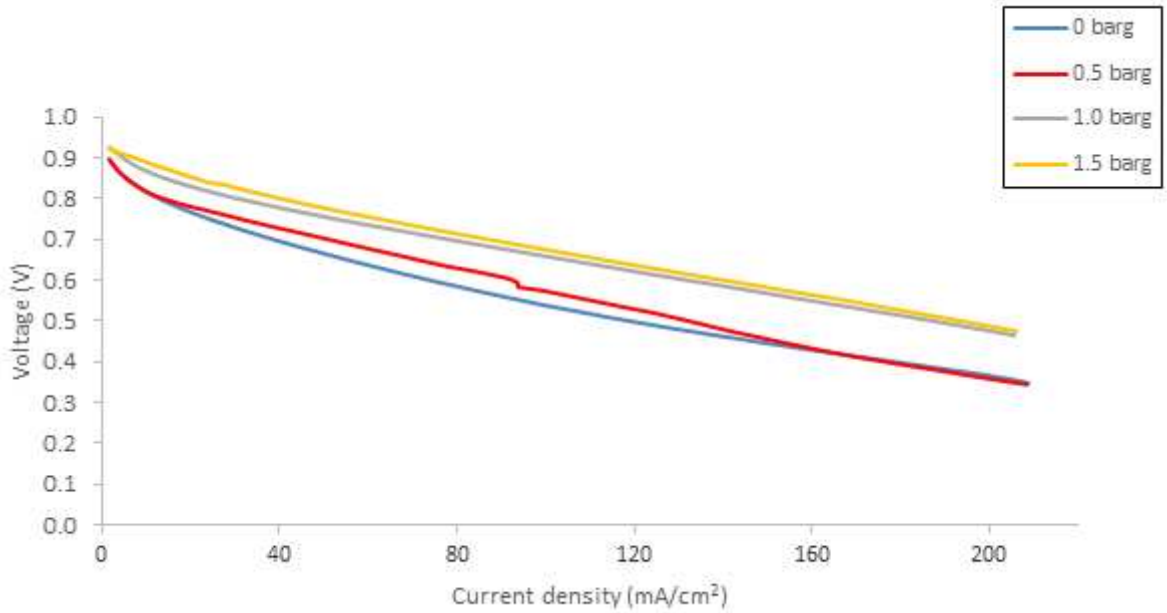
0 barg
0.5 barg
1.0 barg
1.5 barg
1.0
0.9
0.8
0.7
0.6
0.5
0.4
0.3
0.2
0.1
0.0
Voltage (V)
0
40
80
120
160
200
Current density (mA/cm²)

Fig. 8(b)

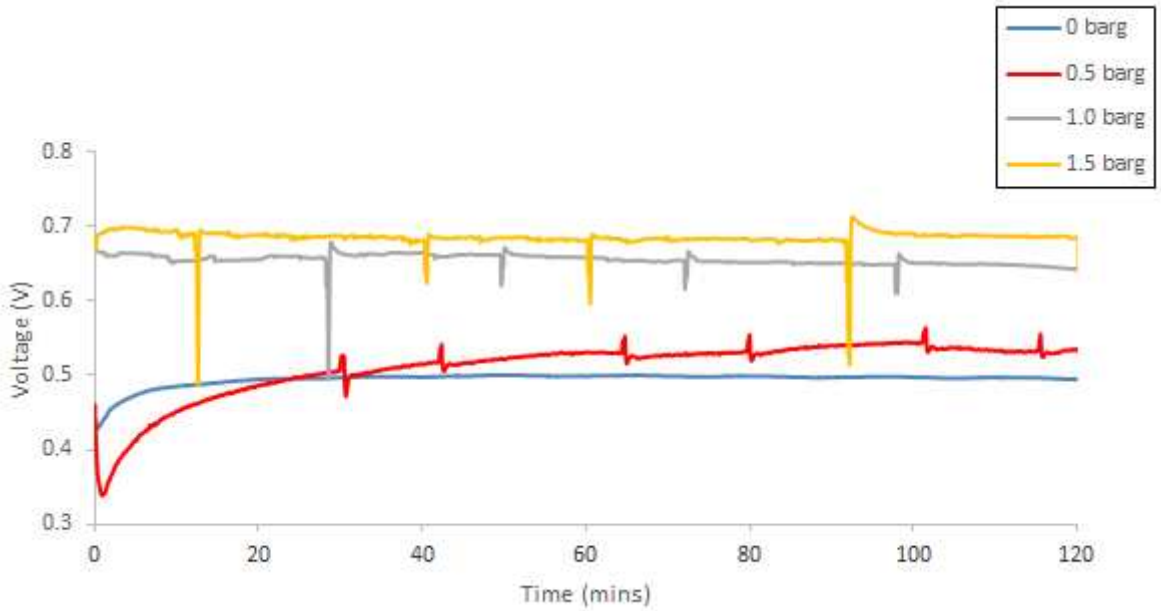
0 barg
0.5 barg
1.0 barg
1.5 barg
Voltage (V)
0.8
0.7
0.6
0.5
0.4
0.3
0
20
40
60
80
100
120
Time (mins)

Fig. 9(a)

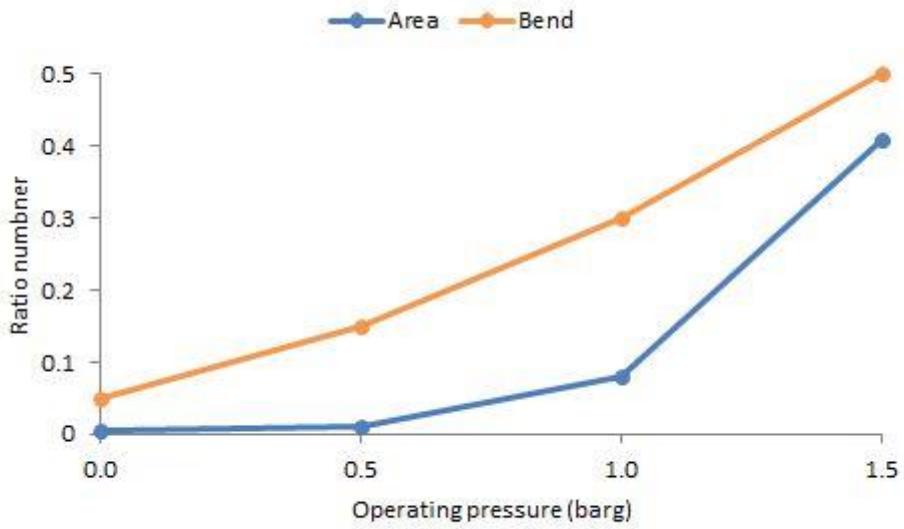
Area
Bend
0.5
0.4
0.3
0.2
0.1
0
Ratio numbner
0.0
0.5
1.0
1.5
Operating pressure (barg)

Fig. 9(b)

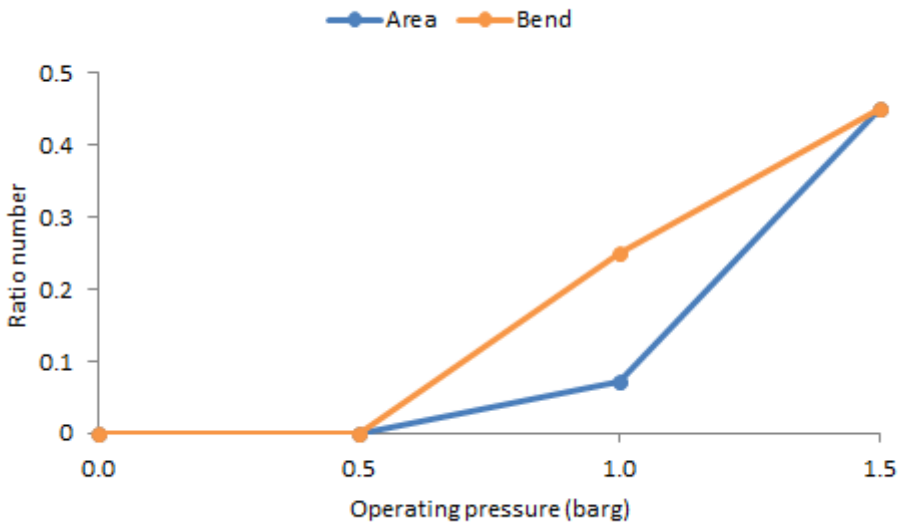
Area
Bend
0.5
0.4
0.3
0.2
0.1
0
Ratio number
0.0
0.5
1.0
1.5
Operating pressure (barg)

Fig. 10(a)

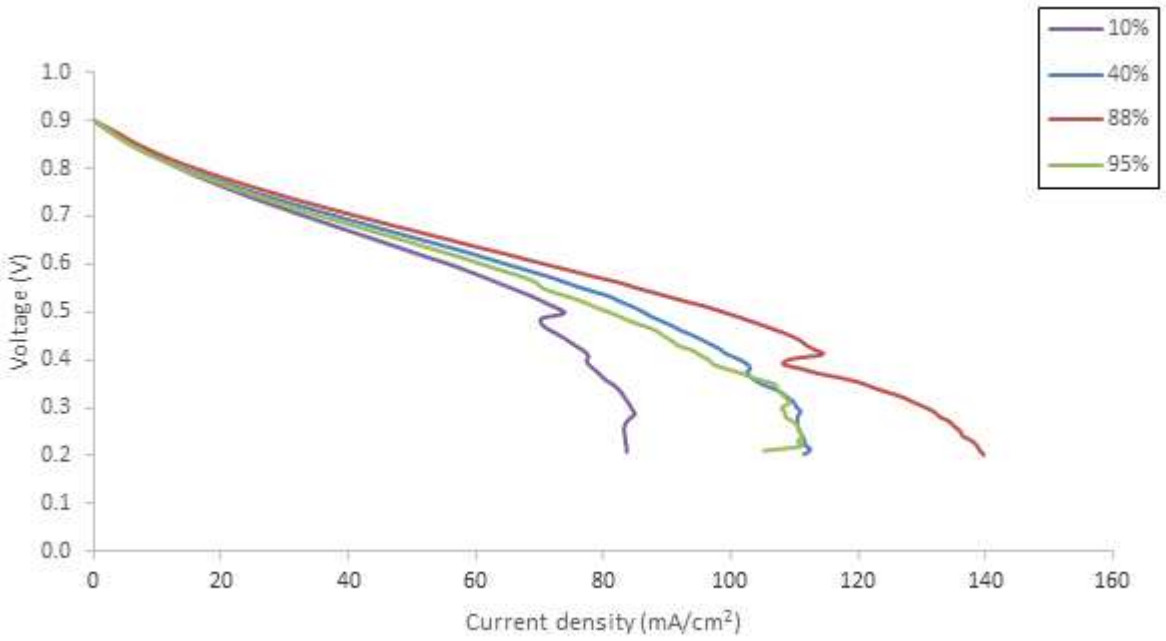
10%
40%
88%
95%
1.0
0.9
0.8
0.7
0.6
0.5
0.4
0.3
0.2
0.1
0.0
Voltage (V)
0
20
40
60
80
100
120
140
160
Current density (mA/cm²)

Fig. 10(b)

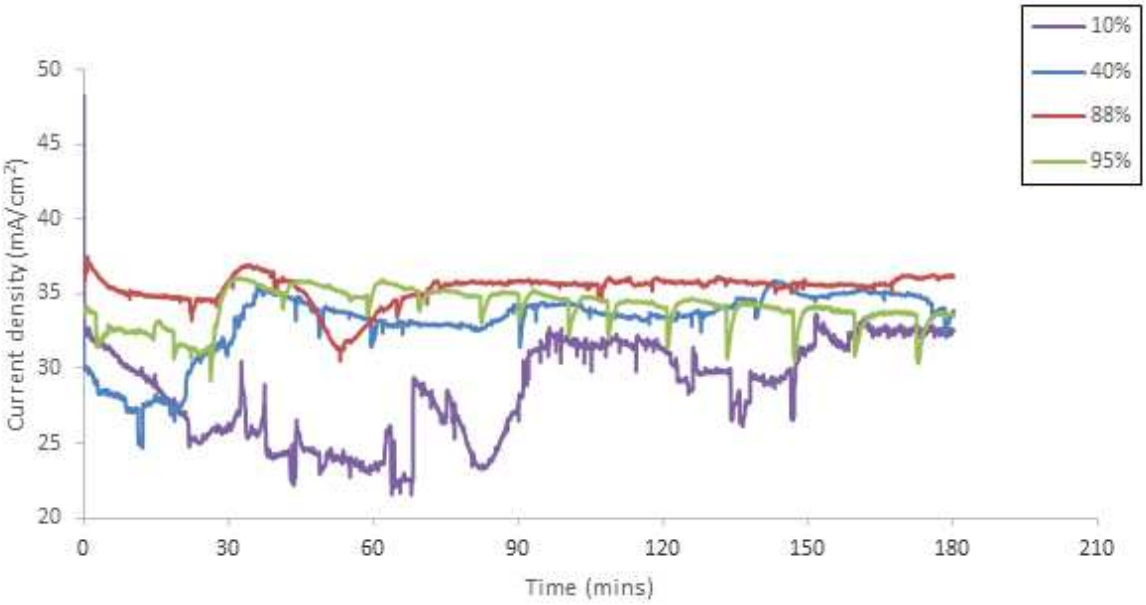
10%
40%
88%
95%
50
45
40
35
30
25
20
Current density (mA/cm²)
0
30
60
90
120
150
180
210
Time (mins)

Fig. 11(a)

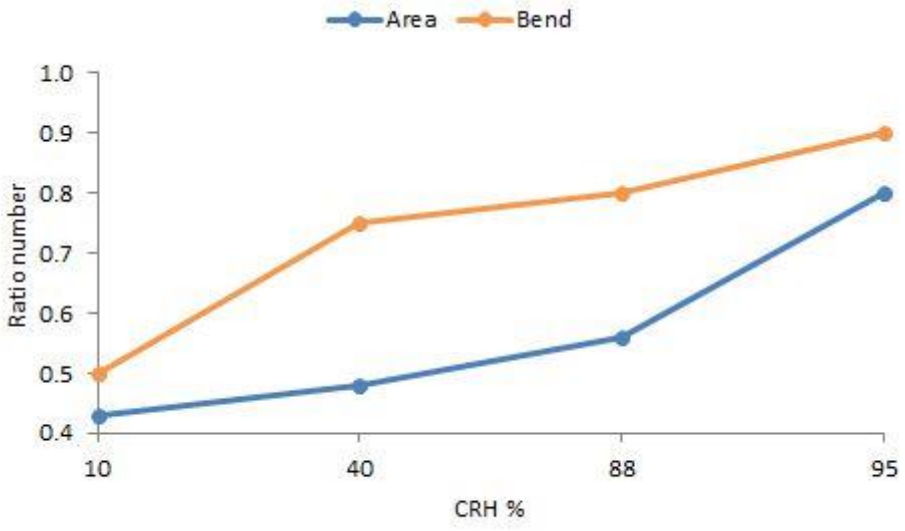

Fig. 11(b)

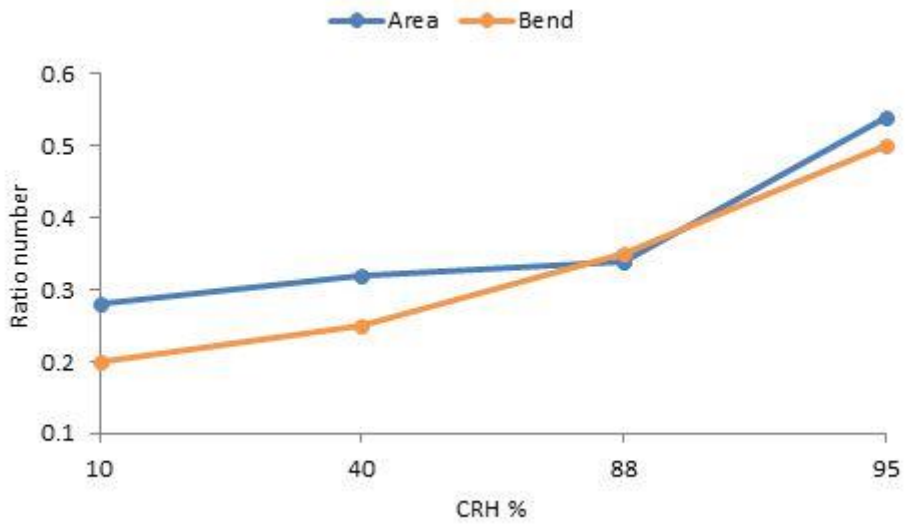

Fig. 12(a)

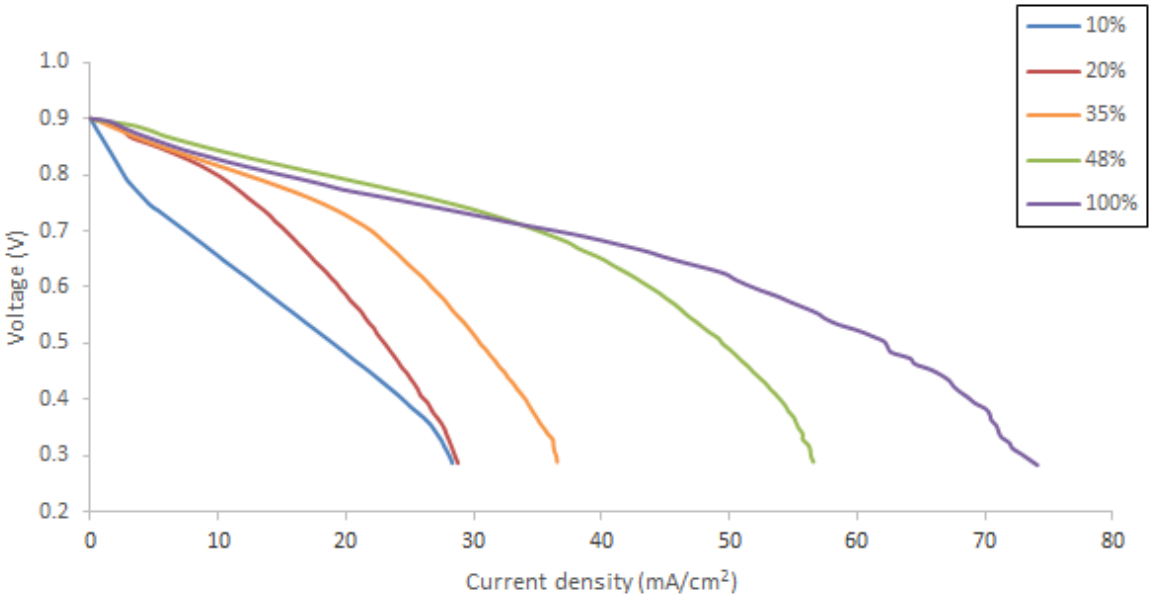
10%
20%
35%
48%
100%
1.0
0.9
0.8
0.7
0.6
0.5
0.4
0.3
0.2
Voltage (V)
0
10
20
30
40
50
60
70
80
Current density (mA/cm²)

Fig. 12(b)

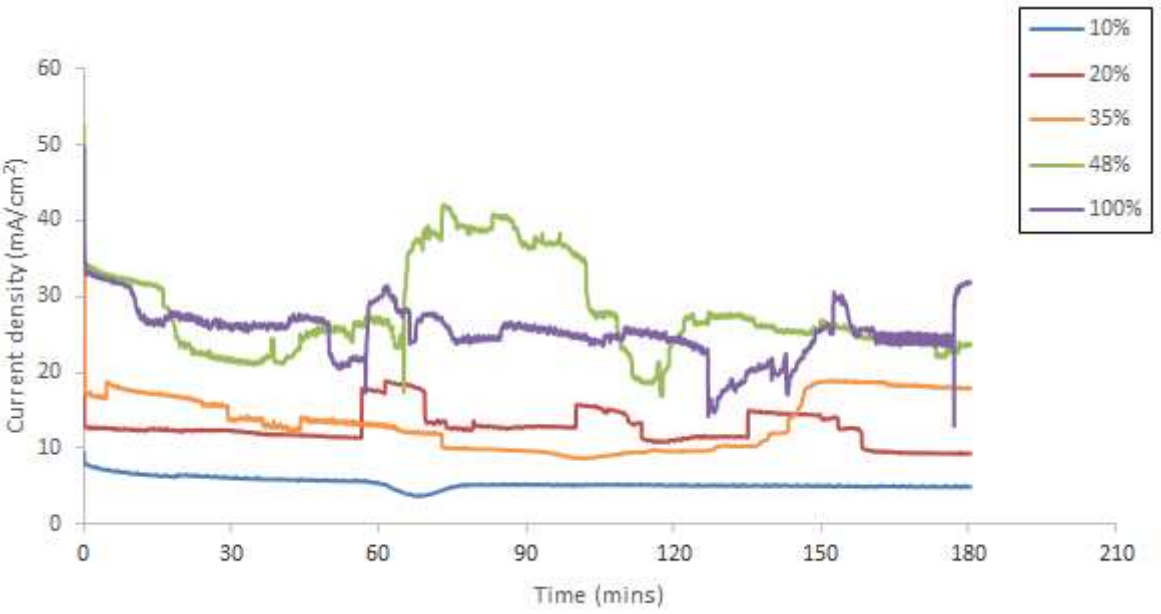
10%
20%
35%
48%
100%
Current density (mA/cm²)
0
10
20
30
40
50
60
0
30
60
90
120
150
180
210
Time (mins)

Fig. 13(a)

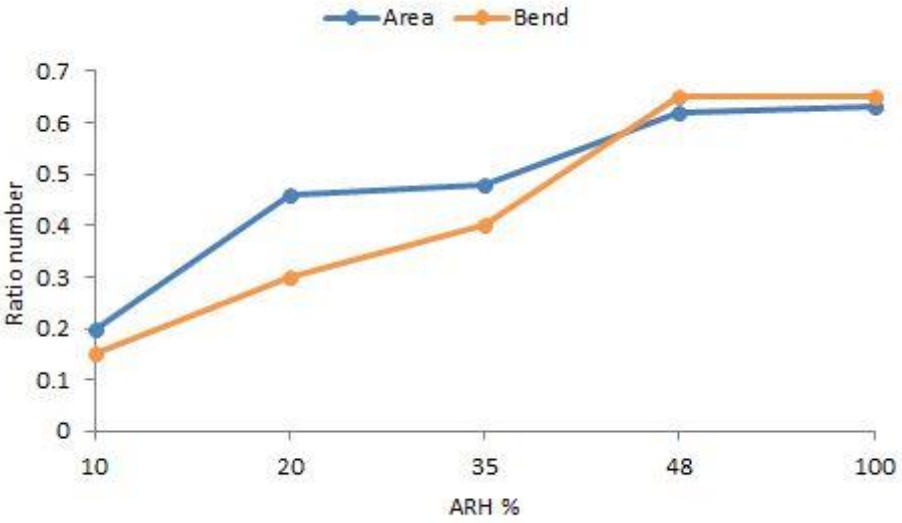

Fig. 13(b)